INSTITUTE OF PHYSICS PUBLISHING JOURNAL OF PHYSICS D: APPLIED PHYSICS
J. Phys. D: Appl. Phys. **37** (2004) 140–150 PII: S0022-3727(04)68775-4

Probing unknown welding parameters from convective heat transfer calculation and multivariable optimization

A De and T DebRoy

Department of Materials Science and Engineering, Pennsylvania State University, PA 16802, USA

Received 11 September 2003
Published 10 December 2003
Online at stacks.iop.org/JPhysD/37/140 (DOI: 10.1088/0022-3727/37/1/023)

Abstract
Values of several parameters that affect calculation of heat transfer during fusion welding such as the arc efficiency, arc radius and the effective thermal conductivity of the liquid metal are not always readily available. Following an inverse approach, a smart model that embodies an iterative procedure for the optimization of multiple unknown variables within the framework of phenomenological laws that govern heat transfer and fluid flow in the weld pool is developed. The optimization scheme considers the sensitivity of computed weld geometry with the unknown parameters. The weld penetration was found to be sensitive to all the unknown variables considered. The weld width was influenced mainly by the arc efficiency and the arc radius. The initial values of the unknown variables did not affect their optimum values but affected the number of iterations necessary for convergence. The model could correctly learn values of multiple unknown parameters from only a few measurements of weld penetration and width and, based on the knowledge of these parameters, provided realistic predictions of heat transfer, fluid flow and weld geometry.

1. Introduction

In the previous two decades, application of transport phenomena has resulted in improved understanding of fusion welding processes and welded materials [1–3]. For example, numerical calculations of heat transfer and fluid flow in welding have enabled accurate quantitative calculations of thermal cycles and fusion zone geometry [4–7]. In many simple systems, the computed thermal cycles have been used to quantitatively understand weld metal phase composition [8–10], grain structure [10, 11], inclusion structure [12–14] and weld metal composition changes owing to both vaporization of alloying elements [15, 16] and dissolution of gases [17, 18]. Capabilities to quantitatively understand geometry, composition and structure of welds in simple systems have provided hope that one day welding engineers may be able to use numerical models to tailor weldment characteristics according to specifications. In reality, the numerical heat transfer and fluid flow codes for fusion welding have so far been used mostly as a research tool [19–21] rather than as a tool for design and manufacturing in the industry. There are several reasons for the restricted use of these advanced tools. An important difficulty is the need for several input parameters that cannot be easily specified based on scientific principles.

Current computer models for the calculation of heat transfer and fluid flow in fusion welding require many input parameters to define the welding system such as the system geometry, welding variables and thermophysical data. Several of these parameters such as the welding current, voltage and welding speed can be easily specified with a reasonable degree of certainty. In contrast, for gas tungsten arc welding process, values of five parameters cannot always be assigned easily. These unknown parameters are: arc efficiency, arc radius, power distribution parameter, the effective thermal conductivity and the effective viscosity of the liquid metal. Although the values of arc efficiency have been experimentally measured for many welding conditions, the reported values vary significantly even for apparently similar welding conditions, reflecting the complexity of the welding process. Measured values of the arc radius and power distribution parameter depend on welding conditions and, as

 © 2004 IOP Publishing Ltd Printed in the UK

a result, their values cannot be ascertained with confidence except for certain narrow windows of welding conditions. Values of the effective thermal conductivity and effective viscosity are important, since they allow accurate modelling of the high rates of transport of heat and mass in systems with strong fluctuating velocities that are inevitable in small weld pools with very strong convection currents. The values of effective conductivity and viscosity are properties of the specific welding system and not inherent physical properties of the liquid metal [19, 21–23]. The results obtained from the numerical heat transfer and fluid flow models depend significantly on the values of these five variables. Although the values of these variables are often assigned from past experience, currently there is no unified basis to accurately prescribe the values of these variables based on scientific principles. A recourse is to develop a modelling procedure utilizing the power of a phenomenological heat transfer and fluid flow model to calculate the optimum values of the five unknown variables from a limited number of experiments. These unknown values can then be used in a numerical heat transfer and fluid flow model under similar welding conditions.

Three optimization algorithms are commonly utilized for parameter estimation. They are the Levenberg–Marquardt method, conjugate gradient technique and conjugate gradient method with adjoint problem. These methods have been discussed elsewhere [24–26]. The Levenberg–Marquardt technique is widely used for the estimation of optimum single values of several unknown parameters and involves optimization of variables by nonlinear least square technique. The conjugate gradient technique utilizes minimization of an appropriately constructed objective function through an iterative procedure. A suitable step size is taken for each iteration along a direction of descent in order to minimize the objective function. The direction of descent is obtained as a linear combination of the negative gradient direction at the current iteration and the direction of the descent of the previous iteration. The conjugate gradient method with adjoint problem is utilized if the unknown parameters can be expressed in terms of the coefficients of a known trial function. This method uses a Lagrange multiplier, and does not require calculation of the sensitivity matrix that is inherent in both the Levenberg–Marquardt method and the conjugate gradient technique. Since the Levenberg–Marquardt method is suitable for the determination of optimum values of several variables, this technique is used in the research reported in this paper.

The optimization schemes for the estimation of unknown parameters in fusion welding are computationally very intensive since they require multiple runs of the phenomenological heat transfer and fluid flow model. As a result, similar efforts reported so far [27–31] have been based on a rather simple heat conduction equation, often utilizing Rosenthal's analytical solution [30, 31] that completely ignored convection in the weld pool. Furthermore, the primary focus of these works was to determine the distribution of heat flux at the work-piece surface exposed to an arc or a laser beam from measured temperatures at several monitoring locations in the solid region. It seems that the adaptation of the simplified heat conduction equation in the previous works was mandated, at least to a large extent, because of the lack of advanced software necessary to rigorously analyse heat and fluid flow in the weldment. With the advances in the computational hardware and software in recent years, it is now possible to undertake computationally intensive optimization schemes that embody realistic three-dimensional numerical heat transfer and fluid flow calculations.

Table 1. Welding variables and experimentally measured weld penetration and width [37].

				Experimental value	
Data set index	Voltage (V)	Current (A)	Weld velocity (mm s^{-1})	Penetration (mm)	Weld width (mm)
1	15.2	200	8.33	1.46	4.61
2	16.5	250	8.33	1.11	5.17
3[a]	16.5	250	6.25	1.38	5.97
4	14.2	200	4.17	1.85	4.90
5	16.5	250	4.17	1.65	6.76

[a] Interpolated data, not directly measured.

The approach adopted here is inherently different from the neural network technique where the input and output variables are related through a set of hidden nodes and their relationship does not have to comply with any physical law. In contrast, when the optimization algorithm embodies a heat transfer and fluid flow model, as adopted in the research reported in this paper, the input welding parameters and the output weld pool geometry are related by a phenomenological framework of the equations of conservation of mass, momentum and energy. In effect, the complete optimization scheme acts as a smart model that identifies few unknown parameters in an iterative manner starting from a set of their initial guessed values exploiting that phenomenological framework. In particular, five unknown welding parameters are estimated through a smart phenomenological modelling approach which includes a combination of the Levenburg–Marquardt method of nonlinear parameter optimization, a numerical heat transfer and fluid flow model and a set of experimentally measured weld pool penetration and width (table 1). The optimization algorithm minimizes the error between the predicted and the experimentally observed penetration and the weld width of a GTA weld pool by considering the sensitivity of the weld penetration and width to each of the unknown parameters.

2. Heat transfer and fluid flow simulation

The flow of liquid metal in the weld pool in three-dimensional Cartesian coordinate system is represented by the following momentum conservation equation [4, 32]:

$$\rho\frac{\partial u_j}{\partial t}+\rho\frac{\partial(u_iu_j)}{\partial x_i}=\frac{\partial}{\partial x_i}\left(\mu\frac{\partial u_j}{\partial x_i}\right)+S_j, \qquad (1)$$

where ρ is the density, t the time, x_i the distance along the $i = 1, 2$ and 3 directions, u_j the velocity component along the j direction, μ the effective viscosity and S_j is the source term for the jth momentum equation and is given as:

$$S_j=-\frac{\partial p}{\partial x_j}+\frac{\partial}{\partial x_j}\left(\mu\frac{\partial u_j}{\partial x_j}\right)-C\left(\frac{(1-f_{\mathrm{L}})^2}{f_{\mathrm{L}}^3+B}\right)u_j+Sb_j, \qquad (2)$$

where p is the pressure, f_{L} the liquid fraction, B a constant introduced to avoid division by zero, and $C(=1.6\times10^4)$ is

a constant that takes into account mushy zone morphology and Sb_j represents both the electromagnetic and buoyancy source terms. The third term on the rhs represents the frictional dissipation in the mushy zone according to the Carman–Kozeny equation for flow through a porous media [33, 34]. The value of the effective viscosity in equation (1) is a property of the specific welding system and not an inherent property of the liquid metal. Typical values of effective viscosity are much higher than that of the molecular viscosity [35, 36]. The higher value is important, since it allows accurate modelling of the high rates of transport of momentum in systems with strong fluctuating velocities that are inevitable in small weld pools with very strong convection currents [22, 36]. The pressure field was obtained by solving the following continuity equation simultaneously with the momentum equation:

$$\frac{\partial(\rho u_i)}{\partial x_i} = 0. \tag{3}$$

The total enthalpy H is represented by a sum of sensible heat h and latent heat content ΔH, i.e. $H = h + \Delta H$, where $h = \int C_p \, \mathrm{d}T$, C_p the specific heat, T the temperature, $\Delta H = f_\mathrm{L} L$, L is the latent heat of fusion and the liquid fraction f_L is assumed to vary linearly with temperature in the mushy zone [4]:

$$f_\mathrm{L} = \begin{cases} 1, & T > T_\mathrm{L}, \\ \dfrac{T - T_\mathrm{S}}{T_\mathrm{L} - T_\mathrm{S}}, & T_\mathrm{S} \leqslant T \leqslant T_\mathrm{L}, \\ 0, & T < T_\mathrm{S}, \end{cases} \tag{4}$$

where T_L and T_S are the liquidus and solidus temperature, respectively. The thermal energy transport in the weld workpiece can be expressed by the following modified energy equation [30]:

$$\rho\frac{\partial h}{\partial t} + \rho\frac{\partial(u_i h)}{\partial x_i} = \frac{\partial}{\partial x_i}\left(\frac{k}{C_p}\frac{\partial h}{\partial x_i}\right) - \rho\frac{\partial(\Delta H)}{\partial t} - \rho\frac{\partial(u_i \Delta H)}{\partial x_i}, \tag{5}$$

where k is the thermal conductivity. In the liquid region, the value of the thermal conductivity in equation (5) is taken as the effective thermal conductivity which is a property of the specific welding system and not an inherent property of the liquid metal. Typical values of effective thermal conductivity are much higher than that of the thermal conductivity of the liquid. The higher value is important, since it allows accurate modelling of the high rates of transport of heat in systems with strong fluctuating velocities that are inevitable in small weld pools with very strong convection currents [34]. Since the weld is symmetrical about the weld centre line only half of the workpiece is considered. The weld top surface is assumed to be flat. The velocity boundary condition is given as [4]:

$$\begin{aligned} \mu\frac{\partial u}{\partial z} &= f_\mathrm{L}\frac{\mathrm{d}\gamma}{\mathrm{d}T}\frac{\partial T}{\partial x}, \\ \mu\frac{\partial v}{\partial z} &= f_\mathrm{L}\frac{\mathrm{d}\gamma}{\mathrm{d}T}\frac{\partial T}{\partial y}, \\ w &= 0, \end{aligned} \tag{6}$$

where u, v and w are the velocity components along the x, y and z directions, respectively, and $\mathrm{d}\gamma/\mathrm{d}T$ is the temperature coefficient of surface tension. As shown in equation (6), the u and v velocities are determined from the Marangoni effect. The w velocity is equal to zero since there is no flow of liquid metal perpendicular to the pool top surface. The heat flux at the top surface is given as:

$$k\frac{\partial T}{\partial z} = \frac{dQ\eta}{\pi r_\mathrm{b}^2}\exp\left(-\frac{d(x^2+y^2)}{r_\mathrm{b}^2}\right) - \sigma\varepsilon(T^4 - T_\mathrm{a}^4) - h_\mathrm{c}(T - T_\mathrm{a}), \tag{7}$$

where r_b is the arc radius of a circular region within which the arc power is focused, d the dimensionless arc power distribution factor which determines the nature of distribution of the power density of the arc, Q the total arc power, η the arc efficiency, σ the Stefan–Boltzmann constant, h_c the heat transfer coefficient and T_a is the ambient temperature. The first term on the rhs is the heat input from the heat source, defined by a Gaussian heat distribution. The second and third terms represent the heat loss by radiation and convection, respectively. The boundary conditions are defined as zero flux across the symmetric surface (i.e. at $y = 0$) as:

$$\frac{\partial u}{\partial y} = 0, \qquad v = 0, \qquad \frac{\partial w}{\partial y} = 0, \tag{8}$$

$$\frac{\partial h}{\partial y} = 0. \tag{9}$$

At all other surfaces, temperatures are set at ambient temperature and the velocities are set to be zero.

3. Optimization procedure

The Levenberg–Marquardt optimization procedure involves minimization of an objective function that depicts the difference between the computed and measured values. For example, if the penetration and width of the fusion zone are of interest, an objective function, $O(f)$, can be defined as follows:

$$\begin{aligned} O(f) &= \sum_{m=1}^{M}\left[\frac{p_m^\mathrm{c} - p_m^\mathrm{obs}}{p_m^\mathrm{obs}}\right]^2 + \sum_{m=1}^{M}\left[\frac{w_m^\mathrm{c} - w_m^\mathrm{obs}}{w_m^\mathrm{obs}}\right]^2 \\ &= \sum_{m=1}^{M}[p_m^* - 1]^2 + \sum_{m=1}^{M}[w_m^* - 1]^2, \end{aligned} \tag{10}$$

where p_m^c and w_m^c are the penetration and the width of the weld pool calculated by the numerical heat transfer and fluid flow model, respectively and, p_m^obs and w_m^obs are the corresponding experimentally determined values. Note that, p_m^* and w_m^* are non-dimensional and indicate the extent of over- or under-prediction for penetration and weld width, respectively. The subscript m in equation (10) corresponds to a specific set of welding parameters such as welding voltage, current, welding speed and other variables in a series of M number of different welds. A computed parameter such as computed penetration, p_m^c, indicates that the calculation is done with mth set of welding parameters. Equation (10) bears a strong resemblance to the functional form of least square technique for the minimization of error. Often an experiment is repeated

to ensure reliability and to determine the standard errors in measurements. For example, if each of the M welds are fabricated a multiple number of times, it is possible to assign a standard deviation in the measured values of penetration, σ_{p_m}, and width, σ_{w_m}. These standard deviations can be included in the objective function such that more reliable measurements with small standard deviations get a higher weight than less reliable measurements that are characterized by relatively large standard deviations. When every weld is fabricated a multiple number of times, the objective function, $O(f)$, can be redefined as follows.

$$O(f) = \sum_{m=1}^{M} \left[\frac{1}{\sigma_{p_m}} (p_m^* - 1) \right]^2 + \sum_{m=1}^{M} \left[\frac{1}{\sigma_{w_m}} (w_m^* - 1) \right]^2. \quad (11)$$

This definition of the objective function ensures that the more accurate measurements will have greater contribution in the calculation of the objective function. In equations (10) and (11), f refers to a given set of five unknown parameters in non-dimensional forms such that:

$$\{f\} \equiv \{f_1\ f_2\ f_3\ f_4\ f_5\} \equiv \{\eta\ r^*\ d\ k^*\ \mu^*\} \equiv \left\{ \eta\ \frac{r_b}{e_r}\ d\ \frac{k_{eff}}{k_S}\ \frac{\mu}{\mu_{fl}} \right\}. \quad (12)$$

It is to be recognized that in addition to the five variables indicated in equation (12), there are uncertainties in the value of the variables such as the current and voltage we consider as 'known'. These uncertainties are small since variables such as current and voltage can be measured fairly accurately. In equation (12), $e_r, k_S, \mu_{fl}, k_{eff}$ and μ, respectively, refer to electrode radius, thermal conductivity of solid material at room temperature, viscosity of molten iron at 1823 K, effective thermal conductivity and effective viscosity of liquid metal. All unknown parameters included in f are dimensionless. The data used in the calculations are given in table 2. Evidently, $O(f)$ is a function of f since $O(f)$ contains variables p_m^* and w_m^*, which are dependent on the parameters included in f. Assuming that $O(f)$ is continuous and has a minimum value, the optimum values of the five unknowns are obtained by differentiating equation (10) with respect to the five unknown parameters and equating each derivative to zero:

$$\left(\frac{\partial O(f)}{\partial f_i} \right)_{i=1,5} = 2 \left[\sum_{m=1}^{M} (p_m^* - 1) \frac{\partial p_m^*}{\partial f_i} + \sum_{m=1}^{M} \left(w_m^* - 1 \right) \frac{\partial w_m^*}{\partial f_i} \right]_{i=1,5} = 0, \quad (13)$$

where f_i represents any one of the five unknowns in dimensionless form indicated in equation (12). Equation (13) contains partial derivatives of weld width and penetration with respect to all five unknown parameters. These partial derivatives are generally referred as sensitivity of the computed weld width and penetration with respect to the unknown parameters. The values of these sensitivity terms are computed numerically by running the numerical heat transfer and fluid flow code and subsequently, calculating the derivatives. For example, the sensitivity of non-dimensional penetration, p_m^*, with respect to efficiency, η, is calculated from the following relation:

$$\frac{\partial p_m^*}{\partial \eta} = \{p_m^*(\eta + \delta\eta, r^*, d, k^*, \mu^*, \text{other parameters}) - p_m^*(\eta, r^*, d, k^*, \mu^*, \text{other parameters})\}\{\delta\eta\}^{-1}, \quad (14)$$

where $\delta\eta$ is very small compared with η. Expression (14) depicts that each sensitivity term needs two executions of the numerical heat and fluid flow analysis. For convergence, equation (13) calls for both p_m^* and w_m^* to be very close to one. In other words, the calculated p_m^c and w_m^c should be close to the corresponding p_m^{obs} and w_m^{obs} for all M sample welds. Since p_m^c and w_m^c in equation (13) are obtained from the solution of the numerical heat transfer and fluid flow model for a certain set of five unknown parameters, and these unknown parameters do not explicitly appear in equation (13), this equation cannot provide a direct solution for the desired unknown parameters. As shown in appendix, considerable rearrangements of the equations are necessary so that they can serve as a basis for an iterative scheme to evaluate the unknown parameters. The final equations take the following form:

$$[S]\{\Delta f^k\} = -\{S^*\}, \quad (15)$$

where Δf^k are the increments of the f values after k iterations; $[S]$ and $\{S^*\}$ are defined in the appendix by equations (A16) and (A17), respectively. The iterations are continued until the objective functions defined by equation (13) are satisfied. The solution methodology is discussed in detail in the appendix.

Table 2. Data used in the calculations.

Physical property	Value
Liquidus temperature, T_L (K)	1785.0
Solidus temperature, T_S (K)	1745.0
Density of liquid metal, ρ (kg m^{-3})	7.2×10^3
Thermal conductivity of solid, K_S (W m^{-1} K^{-1})	25.08
Specific heat of solid, C_{pS} (J kg^{-1} K^{-1})	702.24
Specific heat of liquid, C_{pL} (J kg^{-1} K^{-1})	806.74
Temperature coefficient of surface tension, $d\gamma/dT$ (N m^{-1} K^{-1})	-0.5×10^{-3}
Coefficient of thermal expansion, β (K^{-1})	1.5×10^{-6}
Viscosity of molten iron at 1550°C, μ_{fl} (kg m^{-1} s^{-1})	6.7×10^{-3}
Radius of tungsten electrode, e_r (mm)	1.0

4. Results and discussion

Obtaining the optimum solutions of the five unknown parameters requires calculation of several sensitivity terms, S_{ij}, defined by equation (A21). These terms indicate the effects of variation of the unknown variables on the dimensionless penetration and weld width. Figures 1(*a*) and (*b*) show that an increase in η enhances both p_m^* and w_m^* significantly. This behaviour is anticipated since an increase in η enhances the total absorbed heat flux, and consequently, the size of the weld pool. The penetration is dictated by the heat transfer in the downward direction. An increase in r^* always reduces the heat flux on the surface and in turn, the conductive heat transfer in the downward direction. Thus, an increase in r^* always reduces penetration leading to shallower welds.

Therefore, p_m^* decreases with the increase in r^* for any given value of η. The manner in which r^* affects dimensionless width, w_m^*, depends on the value of η. Low values of arc efficiency, η, leads to a weak temperature gradient along the weld pool surface. Spreading of arc energy over a larger area resulting from high values of r^* further weakens the temperature gradient, which, in turn, results in weak surface velocities in the radial direction. Consequently, the amount of convective heat transported toward the solid–liquid interface is diminished leading to smaller weld width. However, at high values of η, a strong temperature gradient exists at the surface which leads to strong convective heat transfer toward the weld periphery. A wider distribution of arc energy can now still maintain the strong temperature gradient over a wider area without any appreciable decrease in the effective radial heat transfer. Consequently, the computed weld width increases with r^* when η is sufficiently high. For example, figure 1(b) shows that at high values of η, w_m^* increases as r^* increases from 2.0 to 3.5 while the situation reverses at lower values of η. For all values of current and welding speed investigated, the effects of arc efficiency and dimensionless arc radius on the dimensions of the weld pool were similar to those depicted in figure 1.

Figure 1(a) shows that there are several combinations of η and r^* that can provide $p_m^* = 1$. Similarly, from figure 1(b) it is possible to obtain several combinations of η and r^* that would result in $w_m^* = 1$. However, the same set of η and r^* does not lead to $p_m^* = w_m^* = 1$. Therefore, graphical optimization cannot be relied upon to determine even a set of two values of the unknown parameters, let alone the values of all five variables that needs to be optimized.

Figures 2(a) and (b) show the effects of variation of the arc distribution parameter, d, on p_m^* and w_m^*. It is observed that an increase in d from 0.5 to 1.0 enhances p_m^*. As d is increased further, p_m^* becomes insensitive to d over the entire range of its value. In contrast, w_m^* appears to be insensitive to d. The smaller the value of d, the smaller is the peak energy density and vice versa. In other words, the total heat energy is distributed over a smaller area for $d = 1.0$ than that for $d = 0.5$. Thus, as d is increased from 0.5 to 1.0, the heat flux, and consequently the peak temperature in the weld pool increases. The resulting high temperature gradient enhances the heat transfer by conduction in the downward direction resulting in deeper weld pool. However, the peak temperature does not increase appreciably with further increase in d and therefore, the computed penetration remains roughly constant. As d is increased from 0.5 to 1.0, the total energy tends to be focused near the weld pool centre. However, the surface temperature gradient and the radial convective heat transport increases. Because of these two opposing effects, the computed weld width does not show any appreciable change with d.

Figures 3(a) and (b) show the effect of k^* on p_m^* and w_m^*. As k^* increases from about 1.0 to 7.0, p_m^* increases and w_m^* shows a slight decrease. With further increase in k^*, both p_m^* and w_m^* show very little change. In a weld pool without any surface active elements, the main mechanism of heat transport in the downward direction is conduction. An increase in k^*

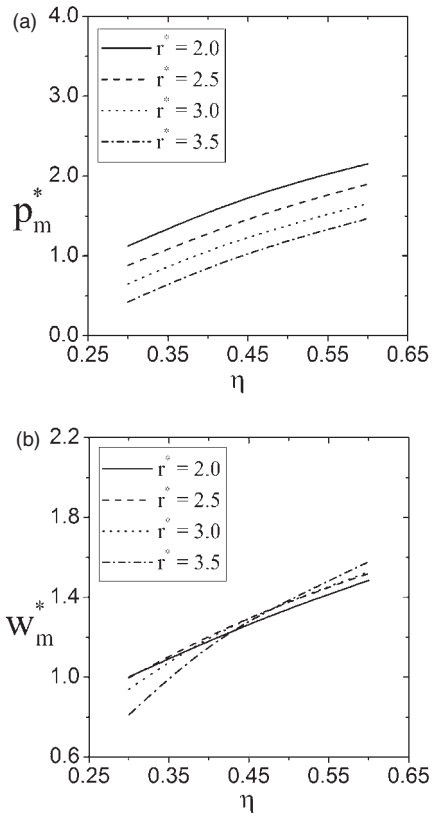

Figure 1. Influence of η on p_m^* and w_m^*. Welding parameters: $I = 250$ A, $V = 16.5$ V, $v = 8.33$ mm s^{-1}, $d = 1.0$, $k^* = 5.02$ and $\mu^* = 7.46$.

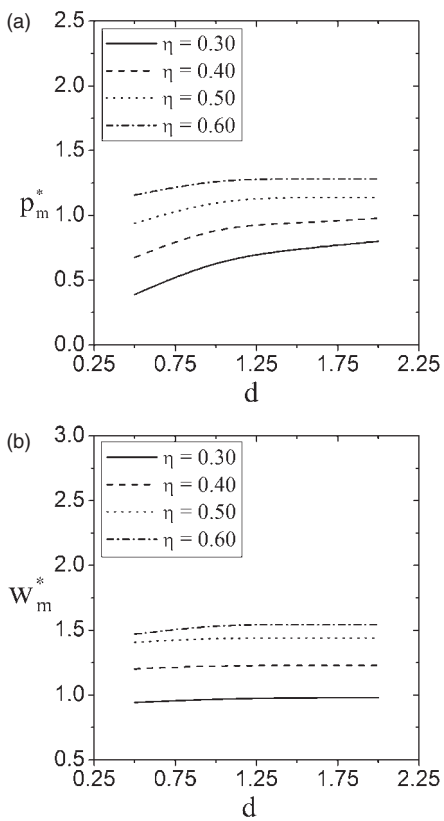

Figure 2. Influence of d on p_m^* and w_m^*. Welding parameters: $I = 200$ A, $V = 14.2$ V, $v = 4.17$ mm s^{-1}, $r^* = 2.0$, $\mu^* = 7.46$ and $k^* = 8.36$.

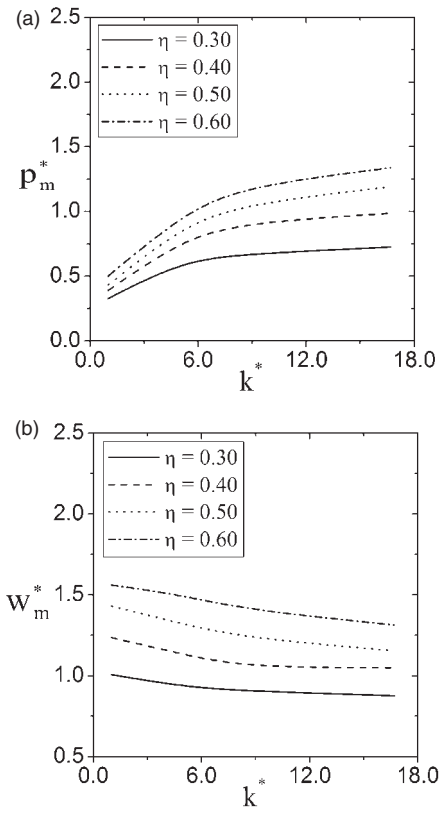

Figure 3. Influence of k^* on p_m^* and w_m^*. Welding parameters: $I = 200$ A, $V = 15.2$ V, $v = 8.33$ mm s^{-1}, $r^* = 2.0$, $d = 1.5$ and $\mu^* = 7.46$.

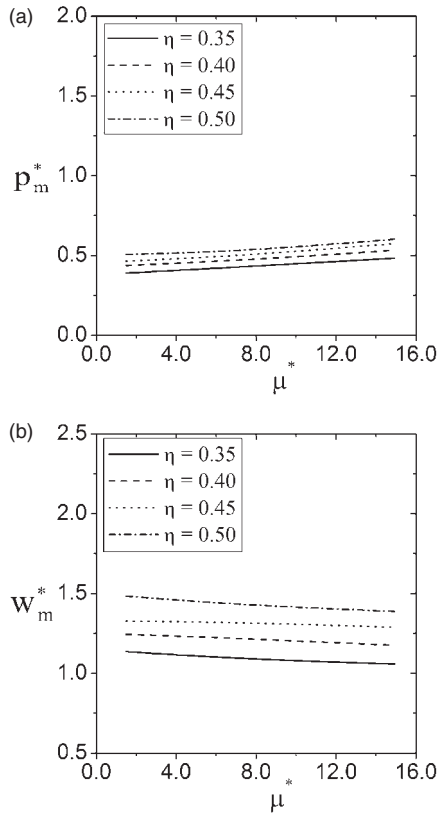

Figure 4. Influence of μ^* on p_m^* and w_m^*. Welding parameters: $I = 200$ A, $V = 15.2$ V, $v = 8.33$ mm s^{-1}, $r^* = 2.0$, $d = 1.0$ and $k^* = 1.67$.

facilitates higher heat conduction. Thus, p_m^* increases with increase in k^*. However, higher values of thermal conductivity also lower the surface temperature gradient. Consequently, the radial convective heat transport is decreased resulting in decreased weld width at higher k^*. As k^* is increased beyond 7.0, the computed weld pool dimensions show very little changes indicating no further enhancement in conductive heat transport.

Figures 4(a) and (b) show that p_m^* increases slightly with increase in μ^* whereas w_m^* shows an opposite effect. For a given temperature gradient, an increase in μ^* reduces surface velocity, since a more viscous fluid flows slowly under the same driving force. The reduced radial convective heat transfer can contribute to the reduction of the weld pool width and slightly higher peak temperature. The slight increase in weld penetration is consistent with the higher peak temperature and enhanced downward conduction heat transfer. When the value of k^* is high, changes in μ^* does not significantly affect the peak temperature. Therefore, the penetration does not change significantly with μ^* at high values of k^* as observed in figure 5(a). Similarly, at high values of k^*, conduction heat transport is important and the changes in μ^* do not affect the weld pool width as observed in figure 5(b).

The results presented so far were required for the construction of sensitivity terms in equation (15). A large volume of numerical calculations of heat transfer and fluid flow are needed to construct the matrix $[S]$ in equation (15) each time an iteration is performed. To start the calculation, a set of initial guessed values are necessary for all the five unknown parameters. When totally random initially guessed values of the unknown parameters were selected, the calculations either failed to converge or resulted in optimized solutions that were not physically meaningful. However, when the values of the unknown parameters were forced to remain within a realistic range of values, the final results converged to one set of optimum values of the unknown parameters for which the objective function attained a minimum value for different initial guessed values of the unknown parameters. Table 3 shows the realistic ranges of the unknown parameters and three sets of initial guessed values of the unknown parameters. Figures 6(a)–(f) show the results of the calculations for three different sets of initial guessed values presented in table 3. The fluctuations in the values of the five unknown parameters with iterations are plotted in figures 6(a)–(e) for the three sets of guessed values. No fluctuation was observed after about 45 iterations for all the parameters. Figure 6(f) shows that the error, $O(f)$, is not reduced beyond 45 iterations. However, there are two typical features worth noting. First, figures 6(a)–(f) show that the nature of fluctuation of all the unknown parameters depends on the choice of their initial values. The fluctuations in the values of all parameters stop after about 20 iterations when the first set of initial values was used. The minimum number of iterations needed for convergence for the second and third sets of initial values was about 35 and 45, respectively. Second, figure 6(e) shows that the starting error is much higher when the third set of initial values was used. As a result, it took more number of iterations to achieve convergence. Thus, the volume of computations

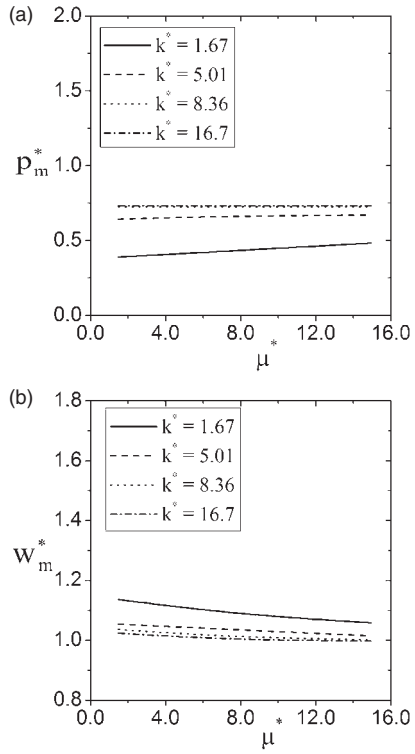

Figure 5. Influence of μ^* on p_m^* and w_m^* for various k^*. Welding parameters: $I = 200$ A, $V = 15.2$ V, $v = 8.33$ mm s^{-1}, $\eta = 0.35$, $r^* = 2.0$ and $d = 1.0$.

Table 3. Various sets of initial guesses for the five unknown parameters.

Unknown parameters (non-dimensional)	Initial guessed values			
	First set	Second set	Third set	Permissible range
η	0.30	0.45	0.60	0.30–0.60
r^*	2.00	2.80	3.50	2.00–3.50
d	0.50	1.25	2.00	0.50–2.50
k^*	1.00	8.33	16.67	1.00–17.00
μ^*	1.49	8.21	14.93	1.00–15.00

needed for optimization depends on the choice of the initial set of guessed values of the unknown parameters. The final optimum values for all the unknown parameters remained same for all three sets of initial values of unknown parameters.

The optimum values of arc efficiency, arc radius, arc distribution parameter, effective thermal conductivity and effective viscosity obtained from the modelling are presented in table 4. Figure 7 shows that the computed values of p_m^* and w_m^* obtained using these optimum values are in fair agreement with the corresponding experimental measurements. However, the predicted penetrations corresponding to the first and fourth measurements (table 1) are relatively lesser in comparison to their measured values. The poor agreement for those two cases may be partially attributed to possible errors in measurements since a fair agreement was observed for all the other predictions. A more detailed comparison between the computed weld pool geometry and the experimentally measured geometry is presented in figure 8. The calculated results also show the temperature contours and the computed velocity field. The computed velocity field shows that the liquid metal is transported from the middle of the pool outwards to the periphery due to negative temperature coefficient of surface tension. These calculated results are consistent with the typical temperature and velocity fields for GTA welds reported in the literature. In the weld pool, heat is transported by a combination of convection and conduction. The relative importance of convection and conduction in the overall transport of heat can be evaluated from the value of Peclet number, Pe, which is defined by:

$$Pe = \frac{u\rho C_p L_R}{k}, \tag{16}$$

where u is the average velocity, L_R the characteristic length taken as the width of the weld pool and ρ, C_p and k are the density, specific heat and thermal conductivity, respectively. When Pe is less than one, the heat transport within the weld pool occurs primarily by conduction. When Pe is much higher than one, the primary mechanism of heat transfer is convection. The order of magnitude of Pe can be easily computed by taking $u = 0.15\,\mathrm{m\,s^{-1}}$, $L_R = 6$ mm, and other parameters from table 2 as about 50. For this value of Pe, the heat is transported within the weld pool mainly by convection.

Although the values of the five unknown parameters determined are valid only for the specific conditions of welding, there are two important reasons for their calculations. First, they are needed for phenomenological modelling, i.e. for the calculation of weld pool geometry and cooling rate using numerical heat transfer and fluid flow model. Second, because of organized research in recent years, there is now a growing quantitative knowledge base for fusion welding, consisting of data, mechanisms, models, rules and laws applicable specifically for fusion welding. Significant expansion of this knowledge base is necessary for it to serve as a basis for the control of welding processes aimed at achieving enhanced reliability and serviceability of welded structures.

5. Summary and conclusions

A smart phenomenological model involving the Levenberg–Marquardt method of parameter estimation and a well-tested three-dimensional numerical model for calculation of heat transfer and fluid flow in the weld pool is developed for the estimation of five unknown welding parameters for GTA welding. A set of experimental data on weld penetration and width for several welding conditions were used to estimate arc efficiency, arc radius, arc distribution parameter, effective thermal conductivity and effective viscosity of the liquid weld metal. The optimization scheme required calculation of how the computed weld geometry was affected by these unknown parameters. The computed weld penetration was found to be sensitive to all these five parameters. The weld width was influenced mainly by arc efficiency and arc radius and, to a much lesser extent, by other parameters. The optimum values of the five unknown parameters were independent of their initial guessed values, although the volume of numerical calculations depended on their initial values. The procedure could correctly estimate the unknown welding parameters

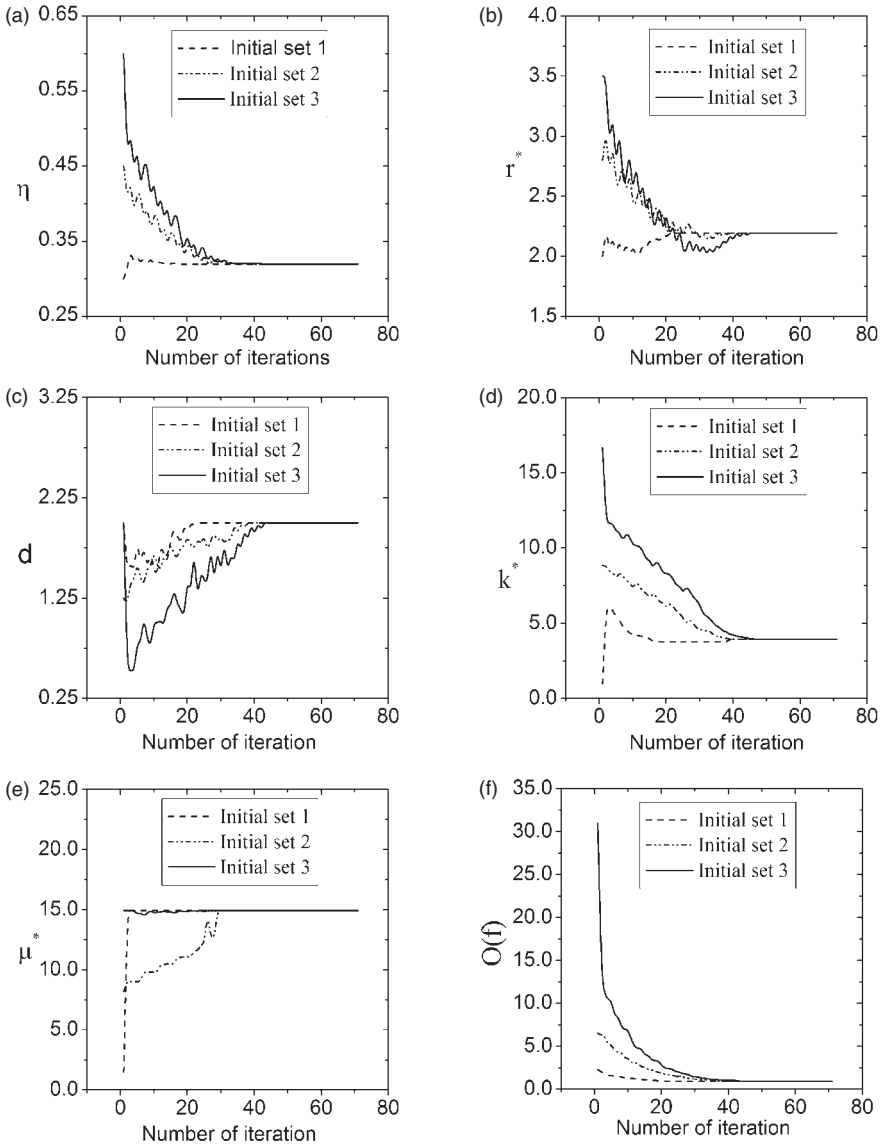

Figure 6. Progress of calculation with three sets of initial guessed values. The guessed values are presented in table 3.

Table 4. Unknown welding parameters determined by the model.

Unknown parameter	Estimated value
Arc efficiency, η	0.33
Arc radius, r_b (mm)	2.2
Arc distribution parameter, d	2.0
Effective thermal conductivity of liquid metal, k_{eff} (W m^{-1} K^{-1})	104.0
Effective viscosity of liquid metal, μ (kg m^{-1} s^{-1})	0.10

based on only a few experimental measurements. The accuracy of the estimated set of the unknown parameters was verified using the numerical heat transfer and fluid flow model and the experimental data. The values of these parameters are useful for numerical heat transfer and fluid flow calculations. Furthermore, the smart phenomenological modelling and its application described in this paper is a contribution to the growing quantitative knowledge base in fusion welding.

Acknowledgments

The work was supported by a grant from the US Department of Energy, Office of Basic Energy Sciences, Division of Materials Sciences, under grant number DE-FGO2-01ER45900. Valuable critical comments from Dr C L Kim and Mr A Kumar are appreciated.

Appendix

In order to explain the basic concept for the optimization in detail, a simplified system involving one dependent variable, p_m^*, measured under three welding conditions is considered first. It is hoped that by explicitly stating all the important steps and avoiding complex symbolic representations, the method can be useful to beginner researchers in the field.

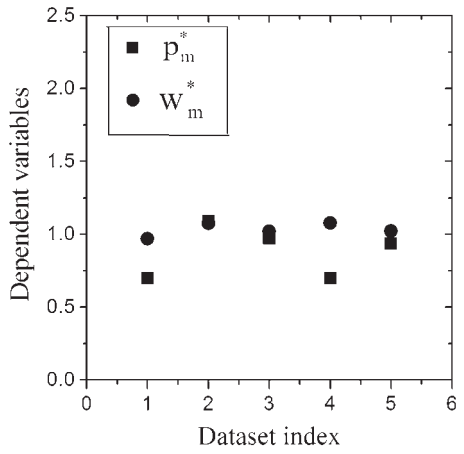

Figure 7. Computed values of p_m^* and w_m^* using the optimized set of five unknown parameters. Data used in the calculations are presented in table 2.

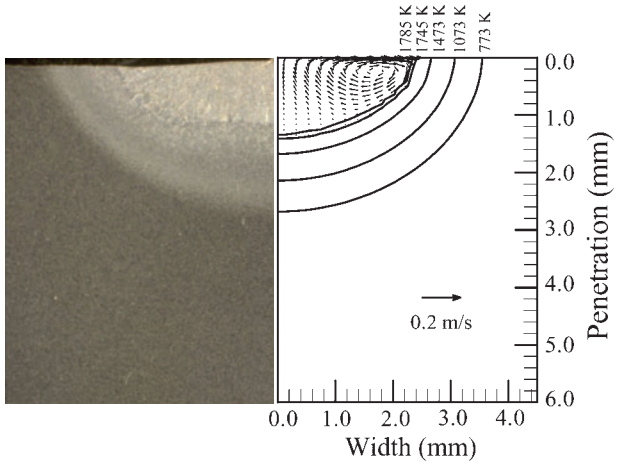

Figure 8. Experimentally determined and computed weld pool geometry. The length of the black arrows show the magnitude of the velocities and the solid lines show the isotherms. Welding variables: $I = 250$ A, $V = 16.5$ V and $v = 8.33$ mm s^{-1} welding speed; other data used in the calculations are given in table 2.

It is further assumed, for simplicity, that there are only two unknown parameters, f_1 and f_2. Finally the application of the methodology to determine five unknown welding parameters is explained. Equation (13) can be written for f_1 and f_2 as:

$$\sum_{m=1}^{3}\left[(p_m^*-1)\frac{\partial p_m^*}{\partial f_1}\right]=0, \tag{A1}$$

$$\sum_{m=1}^{3}\left[(p_m^*-1)\frac{\partial p_m^*}{\partial f_2}\right]=0. \tag{A2}$$

The values of the two unknowns, f_1 and f_2, cannot be directly obtained from the above equations since they do not appear explicitly in these equations. However, the dependent variable p_m^* can be expanded using Taylor's series expansion to explicitly contain values of increments and f_1 and f_2. Considering two successive iterations of p_m^* and taking only the first order terms:

$$(p_m^*)^{k+1}=(p_m^*)^k+\frac{\partial(p_m^*)^k}{\partial f_1}\Delta f_1^k+\frac{\partial(p_m^*)^k}{\partial f_2}\Delta f_2^k, \tag{A3}$$

where Δf_1^k and Δf_2^k are two unknown increments of f_1 and f_2. All other terms on the rhs of equation (A3) are considered to be known. The value of p_m^* at the end of $(k+1)$th iteration, $(p_m^*)^{k+1}$, is unknown since Δf_1^k and Δf_2^k, and hence, f_1 and f_2 after $(k+1)$th iteration are unknown. It should be noted here that p_m^* is always considered to be evaluated through the numerical heat transfer and fluid flow simulation using a corresponding set of f_1 and f_2 and other known parameters.

Equations (A1) and (A2) are rewritten replacing p_m^* by $(p_m^*)^{k+1}$ as:

$$\sum_{m=1}^{3}\left[((p_m^*)^{k+1}-1)\frac{(\partial p_m^*)^{k+1}}{\partial f_1}\right]=0, \tag{A4}$$

$$\sum_{m=1}^{3}\left[((p_m^*)^{k+1}-1)\frac{(\partial p_m^*)^{k+1}}{\partial f_2}\right]=0. \tag{A5}$$

Substituting $(p_m^*)^{k+1}$ by the terms on the rhs of equation (A3), both equations (A4) and (A5) are rewritten as:

$$\sum_{m=1}^{3}\left[\left((p_m^*)^k+\frac{\partial(p_m^*)^k}{\partial f_1}\Delta f_1^k+\frac{\partial(p_m^*)^k}{\partial f_2}\Delta f_2^k-1\right)\times\frac{\partial((p_m^*)^k+(\partial(p_m^*)^k/\partial f_1)\Delta f_1^k+(\partial(p_m^*)^k/\partial f_2)\Delta f_2^k)}{\partial f_1}\right]=0, \tag{A6}$$

$$\sum_{m=1}^{3}\left[\left((p_m^*)^k+\frac{\partial(p_m^*)^k}{\partial f_1}\Delta f_1^k+\frac{\partial(p_m^*)^k}{\partial f_2}\Delta f_2^k-1\right)\times\frac{\partial((p_m^*)^k+(\partial(p_m^*)^k/\partial f_1)\Delta f_1^k+(\partial(p_m^*)^k/\partial f_2)\Delta f_2^k)}{\partial f_2}\right]=0. \tag{A7}$$

Neglecting higher order differentials such as $(\partial/\partial f_1)\times((\partial(p_m^*)^k/\partial f_1)\Delta f_1^k)$, equations (A6) and (A7) are simplified as,

$$\sum_{m=1}^{3}\left[\left((p_m^*)^k+\frac{\partial(p_m^*)^k}{\partial f_1}\Delta f_1^k+\frac{\partial(p_m^*)^k}{\partial f_2}\Delta f_2^k-1\right)\times\frac{\partial(p_m^*)^k}{\partial f_1}\right]=0, \tag{A8}$$

$$\sum_{m=1}^{3}\left[\left((p_m^*)^k+\frac{\partial(p_m^*)^k}{\partial f_1}\Delta f_1^k+\frac{\partial(p_m^*)^k}{\partial f_2}\Delta f_2^k-1\right)\times\frac{\partial(p_m^*)^k}{\partial f_2}\right]=0. \tag{A9}$$

Equations (A8) and (A9) can be rearranged as:

$$\sum_{m=1}^{3}\left[\frac{\partial(p_m^*)^k}{\partial f_1}\frac{\partial(p_m^*)^k}{\partial f_1}\right]\Delta f_1^k+\sum_{m=1}^{3}\left[\frac{\partial(p_m^*)^k}{\partial f_1}\frac{\partial(p_m^*)^k}{\partial f_2}\right]\Delta f_2^k=-\sum_{m=1}^{3}\left[\frac{\partial(p_m^*)^k}{\partial f_1}((p_m^*)^k-1)\right], \tag{A10}$$

$$\sum_{m=1}^{3}\left[\frac{\partial(p_m^*)^k}{\partial f_2}\frac{\partial(p_m^*)^k}{\partial f_1}\right]\Delta f_1^k+\sum_{m=1}^{3}\left[\frac{\partial(p_m^*)^k}{\partial f_2}\frac{\partial(p_m^*)^k}{\partial f_2}\right]\Delta f_2^k=-\sum_{m=1}^{3}\left[\frac{\partial(p_m^*)^k}{\partial f_2}((p_m^*)^k-1)\right]. \tag{A11}$$

Equations (A10) and (A11) can also be expressed as

$$S_{11}\Delta f_1^k + S_{12}\Delta f_2^k = -S_1^p, \tag{A12}$$

$$S_{21}\Delta f_1^k + S_{22}\Delta f_2^k = -S_2^p. \tag{A13}$$

Equations (A12) and (A13) can be expressed in a matrix form as:

$$\begin{bmatrix} S_{11} & S_{12} \\ S_{21} & S_{22} \end{bmatrix} \begin{Bmatrix} \Delta f_1^k \\ \Delta f_2^k \end{Bmatrix} = - \begin{Bmatrix} S_1^p \\ S_2^p \end{Bmatrix} \tag{A14}$$

or

$$[S]\{\Delta f^k\} = -\{S^*\}, \tag{A15}$$

where

$$[S] = \begin{bmatrix} S_{11} & S_{12} \\ S_{21} & S_{22} \end{bmatrix} = \begin{bmatrix} \sum_{m=1}^{3} \frac{\partial (p_m^*)^k}{\partial f_1} \frac{\partial (p_m^*)^k}{\partial f_1} & \sum_{m=1}^{3} \frac{\partial (p_m^*)^k}{\partial f_1} \frac{\partial (p_m^*)^k}{\partial f_2} \\ \sum_{m=1}^{3} \frac{\partial (p_m^*)^k}{\partial f_2} \frac{\partial (p_m^*)^k}{\partial f_1} & \sum_{m=1}^{3} \frac{\partial (p_m^*)^k}{\partial f_2} \frac{\partial (p_m^*)^k}{\partial f_2} \end{bmatrix} \tag{A16}$$

and

$$\{S^*\} = \begin{Bmatrix} S_1^p \\ S_2^p \end{Bmatrix} = \begin{Bmatrix} \sum_{m=1}^{3} \frac{\partial (p_m^*)^k}{\partial f_1} ((p_m^*)^k - 1) \\ \sum_{m=1}^{3} \frac{\partial (p_m^*)^k}{\partial f_2} ((p_m^*)^k - 1) \end{Bmatrix}. \tag{A17}$$

Thus, equations (A1) and (A2) are modified to equation (A14) where the two unknown incremental terms Δf_1^k and Δf_2^k are explicitly defined in terms of known quantities. All other terms in equation (A14) are known at the end of kth iteration. The variables Δf_1^k and Δf_2^k are determined from the solution of equation (A14). The unknown parameters f_1 and f_2 after the $(k+1)$th iteration are obtained from the following relations:

$$\begin{aligned} f_1^{k+1} &= f_1^k + \Delta f_1^k, \\ f_2^{k+1} &= f_2^k + \Delta f_2^k. \end{aligned} \tag{A18}$$

The updated values of f_1^{k+1} and $f_2^{k+1}$are used next to evaluate $(p_m^c)^{k+1}$ through the numerical heat transfer and fluid flow simulation. Next, $O(f)$ is calculated from the following equation:

$$O(f) = \sum_{m=1}^{3} ((p_m^*)^{k+1} - 1)^2 = 0. \tag{A19}$$

The value of $O(f)$ calculated from (A19) is compared with that calculated previously after the kth iteration. Values of f_1 and f_2 are assumed to have converged when the value of $O(f)$ calculated from (A19) after the $(k+1)$th iterations is found to be smaller than a pre-defined small number.

The calculation procedure can be easily extended for any number of unknown variables, if sufficient number of experimental data sets is available. For example, for the five unknown parameters considered in this paper, the expression (A16) is modified as:

$$[S] = \begin{bmatrix} S_{11} & S_{12} & S_{13} & S_{14} & S_{15} \\ S_{21} & S_{22} & S_{23} & S_{24} & S_{25} \\ S_{31} & S_{32} & S_{33} & S_{34} & S_{35} \\ S_{41} & S_{42} & S_{43} & S_{44} & S_{45} \\ S_{51} & S_{52} & S_{53} & S_{54} & S_{55} \end{bmatrix}, \tag{A20}$$

where

$$S_{ij} = \sum_{m=1}^{5} \left(\frac{\partial (p_m^*)^k}{\partial f_i} \frac{\partial (p_m^*)^k}{\partial f_j} + \frac{\partial (w_m^*)^k}{\partial f_i} \frac{\partial (w_m^*)^k}{\partial f_j} \right), \quad \text{for } i, j = 1\text{–}5, \tag{A21}$$

Indices i and j refer to the number of unknown parameters. Furthermore,

$$\{S^*\} = \begin{Bmatrix} S_1^{\mathrm{pw}} \\ S_2^{\mathrm{pw}} \\ S_3^{\mathrm{pw}} \\ S_4^{\mathrm{pw}} \\ S_5^{\mathrm{pw}} \end{Bmatrix} \tag{A22}$$

with

$$S_i^{\mathrm{pw}} = \sum_{m=1}^{5} \left(\frac{\partial (p_m^*)^k}{\partial f_i} ((p_m^*)^k - 1) + \frac{\partial (w_m^*)^k}{\partial f_i} ((w_m^*)^k - 1) \right), \quad \text{for } i = 1\text{–}5. \tag{A23}$$

The unknown matrix $\{\Delta f^k\}$ in equation (A15) has also to be modified as:

$$\{\Delta f^k\} = \begin{Bmatrix} \Delta f_1^k \\ \Delta f_2^k \\ \Delta f_3^k \\ \Delta f_4^k \\ \Delta f_5^k \end{Bmatrix}. \tag{A24}$$

Expression (A18) should now be treated as,

$$\begin{aligned} f_1^{k+1} &= f_1^k + \Delta f_1^k, \\ f_2^{k+1} &= f_2^k + \Delta f_2^k, \\ f_3^{k+1} &= f_3^k + \Delta f_3^k, \\ f_4^{k+1} &= f_4^k + \Delta f_4^k, \\ f_5^{k+1} &= f_5^k + \Delta f_5^k. \end{aligned} \tag{A25}$$

Furthermore, the sensitivity terms such as $\partial (p_m^*)^k / \partial f_i$ or $\partial (w_m^*)^k / \partial f_i$ (for $i = 1\text{–}5$) in expressions (A16) and (A21) often tend to be very small as the values of the unknown parameters f_1, f_2, f_3, f_4 and f_5 move close to the optimum values. As a result, the matrix $[S]$ may tend to become a singular matrix. To avoid any numerical instability, equation (A15) is further modified following Levenburg–Marquardt method as:

$$([S] + \lambda \boldsymbol{I})\{\Delta f^k\} = -\{S^*\}, \tag{A26}$$

where λ is a scalar damping coefficient which is usually taken as 0.001. $\boldsymbol{I}$ is a diagonal matrix defined as [26]:

$$\boldsymbol{I} = \begin{bmatrix} S_{11} & 0 \\ 0 & S_{22} \end{bmatrix}. \tag{A27}$$

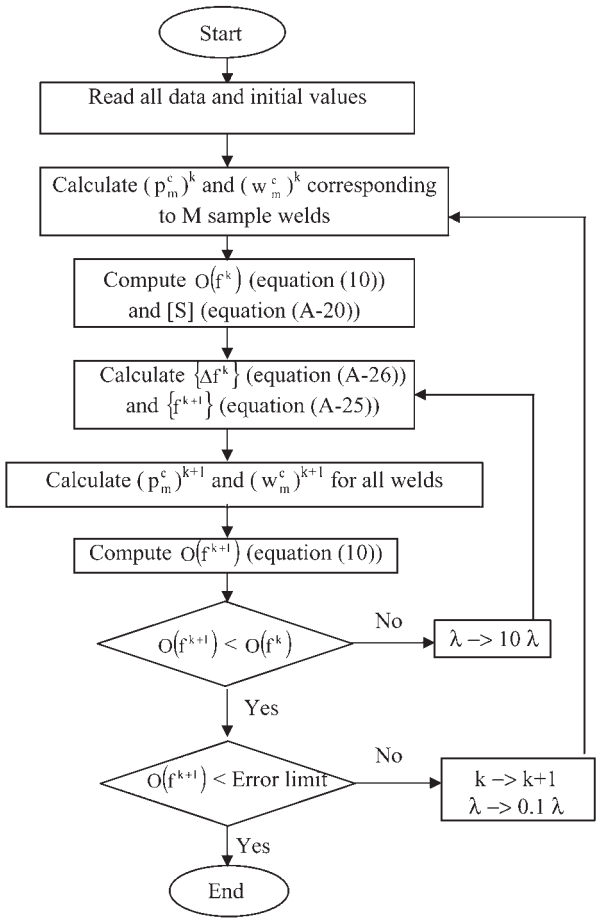

Figure 9. Flow chart of the model.

Hence, equation (A26) can be rewritten as:

$$\left[\begin{bmatrix} S_{11} & S_{12} \\ S_{21} & S_{22} \end{bmatrix} + \lambda \begin{bmatrix} S_{11} & 0 \\ 0 & S_{22} \end{bmatrix}\right] \begin{Bmatrix} \Delta f_1^k \\ \Delta f_2^k \end{Bmatrix} = - \begin{Bmatrix} S_1^p \\ S_2^p \end{Bmatrix}. \quad \text{(A28)}$$

The order of $\boldsymbol{I}$ will always be same as that of the matrix $[S]$. Thus the product $\lambda \boldsymbol{I}$ in equation (A26) ensures that the left-hand term in equation (A26) will remain non-zero even if the determinant of the matrix $[S]$ is zero. The sequence of steps involved in the modelling is shown in figure 9.

References

[1] David S A and DebRoy T 1992 *Science* **257** 497
[2] DebRoy T and David S A 1995 *Rev. Mod. Phys.* **67** 85
[3] Zhao H, White D R and DebRoy T 1999 *Int. Mater. Rev.* **44** 238
[4] Mundra K, DebRoy T and Kelkar K M 1996 *Numer. Heat Transfer* A **29** 115
[5] Elmer W J, Palmer T A, Zhang W, Wood B and DebRoy T 2003 *Acta Mater.* **51** 3333
[6] Kou S and Wang Y H 1986 *Metall. Mater. Trans.* **17** 2265
[7] Pitscheneder W, DebRoy T, Mundra K and Ebner R 1996 *Weld. J.* **75** 71s
[8] Zhang W, Elmer J W and DebRoy T 2002 *Mater. Sci. Eng.* A **333** 320
[9] Cool T and Bhadeshia H K D H 1997 *Sci. Technol. Weld. Joining* **2** 36
[10] Yang Z, Elmer J W, Wang J and DebRoy T 2000 *Weld. J.* **79** 97s
[11] Yang Z, Sista S, Elmer J W and DebRoy T 2000 *Acta Mater.* **48** 4813
[12] Hong T, Pitscheneder W and DebRoy T 1998 *Sci. Technol. Weld. Joining* **3** 33
[13] Babu S S, David S A, Vitek J M, Mundra K and DebRoy T 1995 *Mater. Sci. Technol.* **11** 186
[14] Hong T and DebRoy T 2001 *Ironmaking Steelmaking* **28** 450
[15] Mundra K and DebRoy T 1993 *Metall. Trans.* B **24** 145
[16] Zhao H and DebRoy T 2001 *Metall. Mater. Trans.* B **32** 163
[17] Palmer T A and DebRoy T 2000 *Metall. Mater. Trans.* B **31** 1371
[18] Mundra K, Blackburn J M and DebRoy T 1997 *Sci. Technol. Weld. Joining* **2** 174
[19] He X, Fuerschbach P W and DebRoy T 2003 *J. Phys. D: Appl. Phys.* **36** 1388
[20] Zhao H and DebRoy T 2003 *J. Appl. Phys.* **93** 10089
[21] Zhang W, Roy G G, Elmer J W and DebRoy T 2003 *J. Appl. Phys.* **93** 3022
[22] Paul A and DebRoy T 1988 *Metall. Trans.* B **l9** 851
[23] Hong K, Weckmann D C, Strong A B and Zheng W 2002 *Sci. Technol. Weld. Joining* **7** 125
[24] Beck J V and Arnold K J 1977 *Parameter Estimation in Engineering and Science* (New York: Wiley)
[25] Beck J V, Blackwell B and Clair C R Jr 1985 *Inverse Heat Conduction—Ill-Posed Problems* (New York: Wiley)
[26] Ozisik M N and Orlande H R B 2000 *Inverse Heat Transfer* (New York: Taylor and Francis)
[27] Hsu Y F, Rubinsky B and Mahin K 1986 *J. Heat Transfer, Trans. ASME* **108** 734
[28] Beck J V 1991 *Modeling of Casting, Welding and Advanced Solidification Processes V* ed M Rappaz *et al*, p 503
[29] Rappaz M, Desbiolles J L, Drezet J M, Gandin C A, Jacot A and Thevoz P 1995 *Modeling of Casting, Welding and Advanced Solidification Processes VII* ed M Cross *et al*, p 449
[30] Fonda R W and Lambrakos S G 2002 *Sci. Technol. Weld. Joining* **7** 177
[31] Karkhin V A, Plochikhine V V and Bergmann H W 2002 *Sci. Technol. Weld. Joining* **7** 224
[32] Patankar S V 1982 *Numerical Heat Transfer and Fluid Flow* (New York: Hemisphere Publishing Corporation)
[33] Voller V R and Prakash C 1987 *Int. J. Heat Mass Transfer* **30** 1709
[34] Brent A D, Voller V R and Reid K J 1988 *Numer. Heat Transfer* **13** 297
[35] DebRoy T, Mazumdar A K and Spalding D B 1978 *Appl. Math. Model.* **2** 146
[36] Choo R T C and Szekely J 1994 *Weld. J.* **73** 25s
[37] Dayal A, Harris D, Ion J C and DebRoy T 2003 Department of Materials Science and Engineering, The Pennsylvania State University, University Park, PA, USA, unpublished